



Full Length Article

Assessment of *Ailanthus altissima* seed oil as a potential source for biodiesel production using nickel oxide nanoparticles catalyst

Hammad Ahmad Jan^{a,*}, Ahmed Sadeq Al-Fatesh^{b,*}, Ahmed I. Osman^{c,*}, Igor Surina^d, Fazli Rahim^{a,e}, Ali Sher^f

^a Department of Botany, University of Buner, Swari 19290, Pakistan

^b Chemical Engineering Department, College of Engineering, King Saud University, P.O. Box 800, Riyadh 11421, Saudi Arabia

^c School of Chemistry and Chemical Engineering, Queen's University Belfast, Belfast BT9 5AG, Northern Ireland, UK

^d Department of Wood, Pulp and Paper, Institute of Natural and Synthetic Polymers, Faculty of Chemical and Food Technology, Slovak University of Technology in Bratislava, Radlinského 9, 812 37 Bratislava, Slovakia

^e Department of Botany, Bacha Khan University, Charsadda, Pakistan

^f Department of Agriculture, Bacha Khan University, Charsadda, Pakistan



ARTICLE INFO

Keywords:

Biodiesel
Renewable energy
Biodiesel synthesis
Nanocatalyst synthesis
Novel feedstock

ABSTRACT

The identification of suitable non-edible plant feedstock is crucial not only to meet energy demands but also to be environmentally friendly. This study aimed to synthesize nickel oxide (NiO) nanoparticles and use these for synthesizing biodiesel from the non-edible feedstock *Ailanthus altissima*. The confirmation of NiO synthesis and its characteristics were studied using XRD and SEM. The biodiesel synthesis and its physicochemical characteristics were confirmed using GC-MS, NMR, and FT-IR spectroscopies. The fuel characteristics were examined using ASTM standard procedures. The results confirmed that the nanoparticles were crystalline, spherical to cuboidal in shape, and had an average diameter of 24 nm. The suitable set of parameters for the optimum biodiesel yield (95 %) was the oil-to-methanol ratio of 1:24, 25 mg of catalyst, 60 °C temperature, and a reaction time of 90 min. The majority of the fuel's characteristics fell within ASTM D-6751 acceptable ranges. 14 distinct kinds of FAMES are present, according to the GC-MS results. The FT-IR spectra confirmed the successful synthesis of biodiesel, which displayed significant peaks for several functional groups. ¹H NMR and ¹³C NMR spectrums confirm the conversion of biodiesel synthesis. The environmental friendliness of AAB (*Ailanthus altissima* biodiesel) and its competitiveness as a feedstock for biodiesel production on a commercial scale are confirmed by its physicochemical properties.

1. Introduction

Many issues have emerged as a consequence of industrialization and the continuing rise in the human population that need to be resolved. These include environmental degradation, depletion of fossil resources, and insufficient power supply. In addition to causing environmental issues, including acid pollution, rain, and worse drought conditions due to climate change, excessive fossil fuel usage also leads to the depletion of fuel supplies. Biodiesel is one of the renewable energy sources which is the most suitable alternative to petro-diesel (Suherman et al., 2023;

Osman et al., 2023). Given that the key challenges revolve around conserving the environment and reducing the use of chemicals in fuel production, developing eco-friendly technologies is essential for meeting energy demands and surmounting these obstacles. Consequently, there has been an increasing emphasis on exploring and implementing alternative renewable energy sources, especially biomass (Kour et al., 2019; Chen et al., 2023).

The global trend towards sustainable and renewable energy sources, such as biodiesel, is gaining momentum as it has the potential to meet Pakistan's current and future energy needs. The growing disparity

Abbreviations: AAB, *Ailanthus altissima* biodiesel; NiO, Nickel oxide; FFA, free fatty acid; SEM, scanning electron microscopy; XRD, X-ray Diffraction; H and C-NMR, Nuclear magnetic resonance; GC-MS, Gas Chromatography-Mass Spectrometry; FT-IR spectroscopy, Fourier transform infrared spectroscopy; ASTM, American Society for Testing and Materials; FAME, fatty acid methyl esters; PMDC, Flash Point °C; CP, Cloud Point; PP, Pour Point; HHV, Higher Heating Value.

* Corresponding authors at: School of Chemistry and Chemical Engineering, Queen's University Belfast, David Keir Building, Stranmillis Road, Belfast BT9 5AG, Northern Ireland, United Kingdom.

E-mail addresses: hajmughul@yahoo.com (H. Ahmad Jan), aalfatesh@ksu.edu.sa (A. Sadeq Al-Fatesh), aosmanahmed01@qub.ac.uk (A.I. Osman).

<https://doi.org/10.1016/j.jksus.2023.103084>

Received 30 March 2023; Received in revised form 6 December 2023; Accepted 27 December 2023

Available online 4 January 2024

1018-3647/© 2023 The Author(s). Published by Elsevier B.V. on behalf of King Saud University. This is an open access article under the CC BY license (<http://creativecommons.org/licenses/by/4.0/>).

between the availability and demand of energy is causing Pakistan to experience a serious economic crisis at the moment. The textile, small and medium-sized business, and local transportation industries have already reached a standstill due to the shortage of fuel and electricity. Energy costs are also steadily increasing, and experts predict they will peak by 2050. Moreover, Pakistan's reliance on fossil fuels has led to the import of over 8.1 million tonnes of fuel annually, costing nearly US\$ 9.4 billion. Therefore, to ensure energy security and develop a sustainable energy balance, it is essential to preserve and utilize renewable and sustainable energy resources like biodiesel (Sebayang et al., 2023).

Vegetable seed oil is transesterified using methanol and a catalyst as the principal technique for producing biodiesel (Asif et al., 2017). The catalyst concentration, reaction temperature, and the proportion of oil to methanol principally influence the transesterification process. Homogeneous catalysts are often used in biodiesel manufacturing on an industrial basis (Dawood et al., 2021). Although they provide a higher yield, the larger output is associated with various drawbacks such as excessive methanol utilization (Guldhe et al., 2017), a prolonged neutralization process, cleaning and drying of the biodiesel to remove impurities, catalyst and glycerol. The heterogeneous catalysts for biodiesel synthesis are getting more attention due to their enormous potential. It may streamline the manufacturing and purifying processes and reduce wastewater generation, lowering manufacturing costs, processing equipment, and environmental impacts (Dawood et al., 2021).

Biodiesel is often produced from non-edible oil sources, which may be cultivated on abandoned land and won't be utilized for human food. To circumvent the controversy around the food problem, native non-edible oils are acceptable as an alternative (Bokhari et al., 2019). Some nations use indigenous non-edible oil sources from Karanja, Rubber, Pongame, Peelu, castor, and others to produce biodiesel. Non-edible oil sources may significantly cut carbon emissions when used for biodiesel production. The cultivation of several plant species that produce non-edible oils has spread around the world. With low cost and excellent yield, these plants can withstand harsh weather conditions (Dawood et al., 2021). Many non-edible seed oils are suggested as possible feedstocks to synthesize biodiesel, including *Cannabis sativa*, *Carthamus oxycantha*, *Jatropha curcus*, *Madhuca indica*, *Melia azadarachta*, *Pitachia chinensis*, *Pongamia pinnata* *Raphanus sativus*, *Ricinus communis*, and *Xanthium sibiricum* and others (Asif et al., 2017a,b).

The *Ailanthus altissima* (Mill.) Swingle belongs to the family Simaroubaceae, which is endemic to East Asia and China (Dawood et al., 2021). It belongs to the family Simaroubaceae and is a deciduous tree. Odd, 30–100 cm long, pinnately compound leaves are spirally arranged on the branch of this plant. Each leaf has 10–40 leaflets that are 10–20 cm long. The lanceolate-shaped leaflets have two to four glandular teeth on the margin and are rounded at the base. White diamond-shaped dots or stripes cover the grey bark. Inflorescences with terminally placed flowers vary in colour from yellow to red. The seeds are encased in samaras ranging in colour from yellow to red and are very diverse in size, weight, and thickness depending on the tree's habitat. The seeds are abundant, grouped in groups on trees, and commonly dispersed through the wind. The roots are taproot, which is extensively branched and up to 27 m long. Depending on the geographical region and kind of environment it inhabits, the tree may reach heights of up to 18 to 30 m and can live for an average of 50 years. The flowering maturity arrives at 3–5 years, and the highest seed production is attained at ages 12 to 20. The height and age of the tree affect the number of seed production. An eight-year-old tree may grow to a maximum of 325,000 samaras distributed in 500 clusters. Depending on the season of harvesting and sowing, the seed germination rate is from 64 % to 98 % (Sladonja et al., 2015).

Ailanthus altissima has high ecological tolerance. While surviving a broad variety of temperatures, it is considerably more suited to higher temperatures seen in the temperate zone than lower ones. Due to exposure to low temperatures, seedlings and saplings may not completely grow or do so more slowly due to their high vulnerability to

cold (Sladonja et al., 2015). It can withstand droughts and responds to them in a variety of ways, such as by closing stomata, decreasing hydraulic conductivity in roots, and shifting food reserves from tap roots to lateral roots for when the parent shoot eventually dies, and new shoots need to be produced (Trifilò et al., 2004). The plant can endure various soil conditions, including dry, wet, nutrient-rich, salty, and alkaline soils, as well as clay, sand, calcareous, and gravel substrates. As a result, it has a wide ecological range in terms of soil conditions (Sladonja et al., 2015).

This species is extremely competitive and adaptable to various environmental situations according to its biological and ecological characteristics. It may disperse and establish new seedlings far from the mother plant because of the high percentage of viable seeds it produces and the formation of lateral shoots (Sladonja et al., 2015). Much research has been conducted on *Ailanthus altissima* worldwide, but the literature indicates that not enough is known about the plant's characteristics to support its widespread and effective application in the manufacture of biofuels. Due to the characteristics mentioned, we selected the *Ailanthus altissima* seed oil to produce biodiesel using nickel oxide nanoparticles as a catalyst for the first time. We also studied the physico-chemical properties of synthesized biodiesel. We also synthesized the nickel oxide nanoparticles and studied the physical properties and surface morphology through XRD and other characterizations. The chosen method, transesterification, is not only practical but also cost-effective, making it suitable for large-scale production. Extensive characterization of the produced biodiesel is conducted, comparing its characteristics to ASTM-recommended fuel properties.

2. Materials and methods

2.1. Synthesis of nickel oxide nanoparticles

The method of sol-gel was used to synthesize nickel oxide nanoparticles. The precursor used was Ni(NO₃)₂·6H₂O (nickel nitrate hexahydrate). First, we prepared a 0.1 M solution of nickel nitrate hexahydrate and, second, a 0.02 M solution of citric acid (C₆H₈O₇). Then, the two solutions were mixed under constant stirring at 500 rpm and 80 °C temperature, leading to gel formation. The gel was first dried at 80 °C in an oven, then it was calcined for two hours at 500 °C in a muffle furnace, and last, it was pulverized (Adiba et al., 2020).

2.2. X-ray (XRD) diffraction of the nanoparticles

XRD is a widely used technique to investigate the basic crystallographic properties of solids. For this purpose, the SHIMADZU 6000 diffractometer was used. For maintaining the current at 30 mA and voltage at 40 kV, the diffractometer was equipped with a CuKα (K = 1.54 Å). The data was collected at 2θ within the range of 10°–90°. The nanoparticle size was measured from step size and scan rate at a speed of 10° per minute. Between 10 °C and 60 °C, all measurements were taken. With the help of XRD31 software, the Peak broadening and peak positions were determined. A heterogeneous average diameter of nanoparticles was obtained by completing the calculation using the Scherrer equation (Nath et al., 2020).

$$D = \frac{k\lambda}{\beta\cos\theta} \quad (1)$$

Where

$k = 0.9$ representing the shape factor.

$\lambda = 1.54 \text{ \AA}$ representing the radiation wavelength.

$\beta =$ representing the intensity of FWHM (full width of half of the maximum) radians.

2.3. Nanoparticle scanning electron microscopy (SEM)

For studying the surface morphology of the nanoparticles, SEM was conducted. For this purpose, the JEOL JSM-5910 & HT7800 Ruli model of scanning electron microscope was used. The scanned images were captured using the field emissions from an SEM microscope under a 20 kV accelerating voltage. It made it possible to evaluate catalyst surfaces qualitatively and helped explain events that occurred during pretreatment and calcination.

2.4. Determination of oil contents in the feedstock

The collected seeds were washed thrice with distilled water and then desiccated in a hot air oven at 50 °C. About 25 gm of dried seeds were powdered. 10 gm of seed powder was taken in the thumbnail. As an internal solvent, we used ether. The soxhlet containing the seed powder was run for 8 h at a temperature of 65 °C. The given equation was used for calculating the total oil content (Jan et al., 2022b).

$$W4 = \frac{W3 - W1}{W2} \quad (2)$$

Where W_1 = represents the empty flask weight, W_2 = quantity of the ground seed before the oil is extracted, W_3 = the weight of the flask after the extraction of the oil, and W_4 = represents the amount of oil contents in the feedstock.

2.5. Determining free fatty acid (FFA)

The method of acid-base titration (Jan et al., 2022b) was followed to measure the free fatty acid (FFA) content. With the help of the given equation, the FFA value was determined.

$$FFA\% = \frac{(A - B) \times C}{V} \times 100 \quad (3)$$

Whereas,

A = Used quantity of KOH.

B = Used amount of KOH in blank titration

C = KOH $\frac{g}{L}$ concentration of.

V = Oil sample volume.

2.6. Method of biodiesel synthesis

Due to the low FFA of the feedstock, the transesterification method was followed for the biodiesel synthesis. The percent yield of biodiesel was calculated using the equation given below (Birla et al., 2012).

$$\text{Percentage yield of Biodiesel} = \frac{\text{Biodiesel produced}}{\text{Oilsample used in reaction}} \times 100 \quad (4)$$

2.7. Evaluation of the fuel properties

Following ASTM standards, the fuel properties of the synthesized biodiesel were evaluated (Table 1) (Fadhil et al., 2017).

2.8. Analyzing the physicochemical characteristics of biodiesel

The synthesis of AAB and examination of its physicochemical characteristics have been confirmed by FT-IR, GC-MS, and NMR spectroscopy.

2.8.1. Biodiesel sample NMR spectroscopy

^{13}C - and ^1H NMR spectroscopy was used for confirmation of the biodiesel synthesis. A 600 MHz Avance NEO Bunker spectrometer was used for this purpose. The 5 mm BBF smart probe was equipped with a spectrometer. The data was collected at 21 °C on 11.75 T. Both $\text{Si}(\text{CH}_3)_4$ and chloroform-d were utilized for confirmation as internal standard

Table 1

Fuel properties of the AAB and ASTM standard methods adopted for properties checking.

Fuel Property	ASTM Methods	Test Limit ASTM D6751	AAB (B100%)
Acid value (KOH mg/kg)	ASTM D-664	0.80	0.47
Flash Point °C (PMCC)	D-93	130	78
Density at 15 °C kg/L	D-4052	0.820–0.900	0.893
Kinematic Viscosity at 40 °C cSt	D-445	1.9–6	4.21
Pour Point °C	D-97–12	–15 to 16	–8.6
Cloud Point °C	D-2500–11	–3 to 12	–10.9
Sulphur % wt	D-5453	0.007	0.0007
Calorific Value kJ/kg	D-5865	35,000	27,763
Cetane no.	D-613	45	46
Oxidative stability 110 °C (h)	EN-14112	Mini. 3 h	2.91
Water content (mg/kg)	ASTM D-6304	≤0.05	0.085
Refractive index @ 40 °C	ASTM D-1747	—	1.458
Iodine number mg $\text{I}_2/100$	ASTM D-4607	≤120	81
Higher heating value MJ/kg	ASTM D-240	39–43	41.83
Distillation temperature 90 % recovery	ASTM D-1160–06	360	352
Carbon Residue	ASTM D-4530	0.05	0.04

solvents. 1.0 scans, 8 scans of recycle time, and a pulse length of 30 degrees was used to measure the spectrum for ^1H NMR (300 MHz). The spectrum of the ^{13}C NMR (75 MHz) was measured at 1.89 scans with a 160 scan recycle delay and 300 pulse duration. The conversion of triglycerides to related FAMES was expressed as a percentage of the residual solvent peak. Fourier Transform Infrared (FT-IR) Analysis.

The various functional groups contained in the biodiesel sample were identified using the FT-IR analysis. The different stretching and bending vibrations confirm the presence of various functional groups and biodiesel formation (Uğuz et al., 2019). The infrared spectra for the synthesized biodiesel were obtained using a VARIAN Model-AA280Z FT-IR spectrometer. In the spectrometer, a graphite tube atomizer type GTA-120 was fitted. Each spectrum was collected in a short period of time utilizing 4 scans at a resolution of 4 cm^{-1} . The spectrometry was conducted in the 400 – 4000 cm^{-1} range. To process all of the findings, computer software called Spectrum was employed.

2.8.2. FAMES' qualitative and quantitative study

The GC-MS spectroscopy was conducted to determine the FAMES composition and their quantity in the biodiesel sample. The Shimadzu Japan-made Model QP-2010 Plus GC-MS was used. A 0.1 μL of biodiesel was put into the spectrometer. The solvent C_6H_{14} was employed, and the vector gas helium was used at a 1.44 mL/min rate. Furthermore, the injector and detector temperatures were set to 250 °C, and the column temperature was set in a range of 50 to 300 °C with a flow rate of 80 degrees per minute. The mass spectrograph was programmed to scan between 50 and 1000 m/z using electron impact ionization.

3. Results and discussion

3.1. X-ray diffraction of nickel oxide nanoparticles

XRD is used to determine a material's crystalline phase (Dawood et al., 2021). Monochromatic X-ray interference on crystalline material is a phenomenon that XRD is investigating (Dawood et al., 2021). Fig. 1 clearly shows that the nanoparticles are crystalline. The strong diffraction peaks obtained at 2θ angles of 37.22°, 43.34°, and 62.81° that correspond to the 111, 200, and 220 Miller indices, respectively, confirm the synthesis of nickel oxide nanoparticles and crystalline nature of it (Ghazal et al., 2021). The average diameter of nanoparticles is 24 nm.

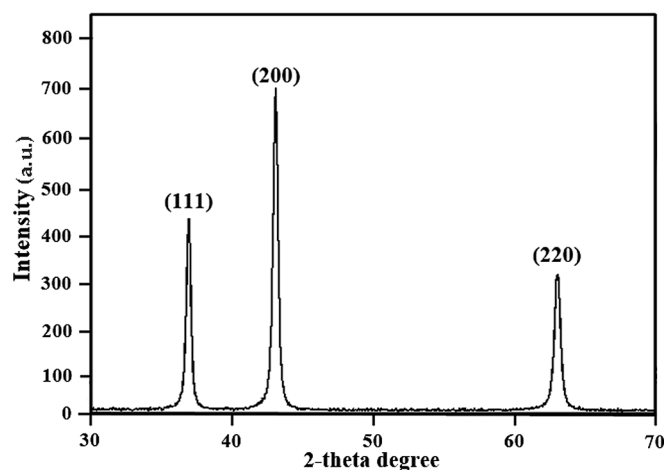


Fig. 1. XRD patterns confirming the NiO nanoparticles synthesis.

3.2. Surface and morphological characteristics study of nanoparticles

We studied the surface and morphological characterizations of the nanoparticles with the help of the SEM Jeol Model JSM-6390LV model. It is clear from Fig. 2 that the particles have spherical to cuboidal symmetry with a smooth surface. The nanoparticles have uniform sizes (Dharmaraj et al., 2006; Ariyanta et al., 2021).

3.3. Determination of oil and FFA contents

The soxhlet method confirmed that the feedstock has 22 % oil content. The acid-base titration method confirmed that the feedstock has an FFA of 0.47 mg KOH/g, less than the ASTM D-6751 standard (Kuepethkaew et al., 2017).

3.4. Parametric optimization of biodiesel yield through transesterification

Because of its simplicity and being economically viable, transesterification is the most convenient method (Rezania et al., 2019). Transesterification is an important step since it may bring the viscosity

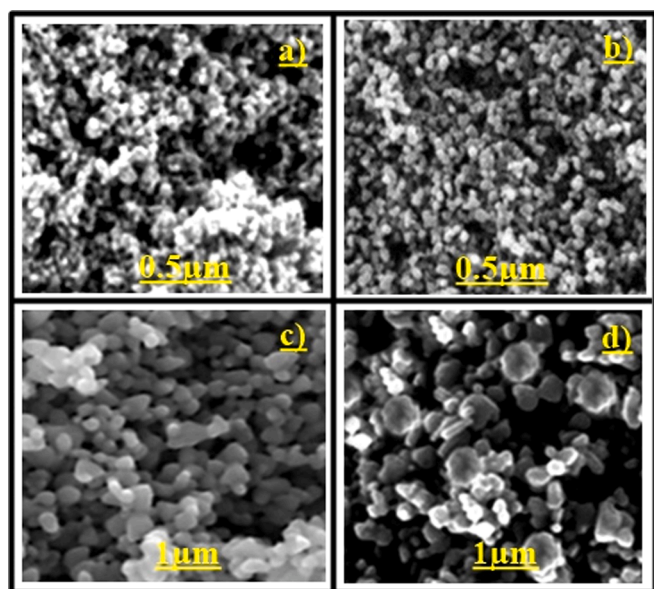


Fig. 2. SEM analysis of NiO nanoparticles to confirm the synthesis of nanoparticles and size, a) 0.5 μm X5,000b) 0.5 μm X10,000; c) 1 μm X10,000; d) 1 μm X20,000.

of the feedstock or vegetable oils closer to that of conventional fuel (Mumtaz et al., 2017). During the transesterification process, a number of variables have been reported to be crucial for obtaining the maximum biodiesel yield, including the oil-to-methanol ratio, catalyst concentration, reaction time, and reaction temperature (Rezania et al., 2019). Therefore, we also conducted a parametric transesterification study to get the optimum biodiesel production (Takase et al., 2014).

3.4.1. Oil to methanol ratio

The yield of biodiesel is significantly affected by the methanol-to-oil ratio, and previous studies show that as methanol concentration increases, so does the yield of biodiesel (Takase et al., 2014; Ullah et al., 2020). Therefore, we also varied the oil-to-methanol ratios as 1:12, 1:18, 1:24, 1:30, and 1:36 to attain the maximum yield. The finding of the current work demonstrates clearly that the maximum biodiesel yield was attained at a ratio of 1:24 oil to methanol (Fig. 3a). Due to the reversibility of the transesterification process, a higher stoichiometric ratio improves the solubility as well as the reactivity of the Me-OH and triglyceride molecules (Tan et al., 2019). Furthermore, a significant quantity of Me-OH is needed to break the bonds between glycerin and fatty acids (Kumar, 2017). Conversely, a high methanol concentration cannot enhance biodiesel output by not only hindering the ester recovery but also raising costs (Ullah et al., 2020).

3.4.2. Catalyst concentration

When a suitable quantity of catalyst is present, the transesterification process proceeds effectively (Encinar et al., 1999; Takase et al., 2014). therefore, the amount of catalyst was kept at 15, 20, 25, 30, and 35 mg to determine the best catalyst concentration at which maximum yield should be obtained. This research shows that a catalyst concentration of 25 mg led to the highest yield (Fig. 3b). As catalyst concentration rises, more active sites become accessible for reactants to be converted into products, resulting in an increase in biodiesel yield and a reduction in reaction time (Srilatha et al., 2009; Jan et al., 2023). Furthermore, a sufficient catalyst concentration lowers the cost of the product by using less energy (Leung and Guo, 2006; Jan et al., 2022a).

3.4.3. Reaction temperature

In order to determine the minimum temperature at which the highest biodiesel production should be attained, we performed transesterification operations at five distinct temperatures of 40, 45, 50, 55, and 60 °C while maintaining the other variables constant. Due to its direct effect on the production of biodiesel as well as the duration of time it takes to react (Yu et al., 2021). In addition, to reduce energy consumption and, therefore, product cost, the transesterification reaction temperature for industrial-scale biodiesel synthesis must be as low as possible. According to our study, the biodiesel yield jumped to 95 % when the temperature was raised from 55 to 60 °C. (Fig. 4a). Since high temperatures reduce the solution's viscosity, increase the reactants' solubility, and speed up the rate at which reactants are transferred to the product, it is clear that the reaction temperature, biodiesel yield, and reaction time all have a significant relationship (Silva and Oliveira, 2014; Barros et al., 2020).

i. Reaction time

As the other factors addressed earlier, the reaction duration is important to biodiesel yield, especially on an industrial scale, since it raises production costs owing to higher energy consumption (Gebremariam and Marchetti, 2018; Dhawane et al., 2018; Barros et al., 2020). The reaction durations were kept at 30, 60, 90, 120, and 150 min in order to establish the minimal optimal reaction time for maximum biodiesel output. 90 min of reaction time resulted in the highest yield (95 %), whereas longer reaction times resulted in no change in yield (Fig. 4b). The same findings have been reported by more studies (Niju et al., 2016; Gebremariam and Marchetti, 2018; Barros et al., 2020;

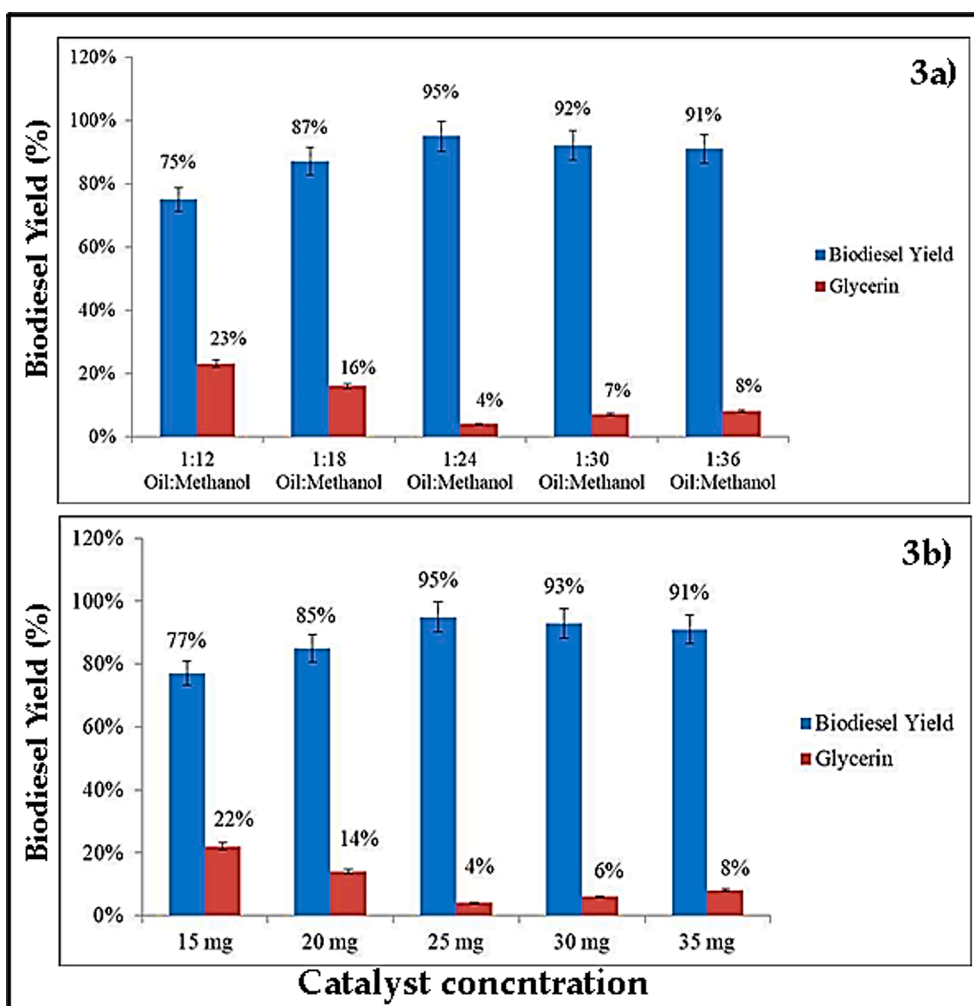


Fig. 3. A) oil to methanol ratio has a positive effect on biodiesel yield and a negative on glycerin formation; b) catalyst concentration has a positive effect on biodiesel yield, but a high concentration of catalyst also favours the formation of more glycerin.

Ullah et al., 2020).

3.5. Fuel properties of biodiesel

The fuel characteristics of biodiesel are mentioned in Table 1. We determined the kinematic viscosity for AAB $4.21 \text{ mm}^2/\text{s}$ at 40°C , which is near to normal diesel and below the ASTM D-6751 required limit (Ullah et al., 2020). The density of 0.893 kg/L is within the parameters set by ASTM D-6751 (Patchimpet et al., 2020). Moreover, the calorific value of 27763 kJ/kg falls below the ASTM D-6751 range. It has a reduced calorific value compared to conventional diesel because of its increased oxygen concentration (Kaisan et al., 2017; Ullah et al., 2020).

AAB has a flash point of 78°C . It is dependent on the methanol level of the biodiesel. Adding 0.5% methanol decreases biodiesel's flash point to 50% (Table 1). Some studies have suggested a flash point for biodiesel of $160\text{--}202^\circ\text{C}$ (Dias et al., 2008; Refaat et al., 2008).

The AAB has a cetane value of 46, which is slightly above the ASTM standard (Table 1). Nitric acid Iso-octyl, in small amounts, can lower the cetane number (Khan et al., 2009; Knothe, 2009). Moreover, the PP and CP values of the synthesized biodiesel are -8.6°C and -10.9°C , respectively (Mofijur et al., 2015). Synthetic biodiesel has sulphur contents of 0.0007 parts per million. It is smaller than ASTM's recommended value. So, the AAB is environmentally friendly biodiesel (Kumar, 2017; Ullah et al., 2020).

The ASTM D-6751 minimal requirement is met by the oxidative stability of AAB, which is 2.91 h . The biodiesels can react with oxygen

even at room temperature. It demonstrates the relative sensitivity of fuel the oxidative degradation (Pullen and Saeed, 2012). Thus, the oxidation susceptibility of biodiesel is advantageous for the environment (Chrysi-kou et al., 2022); however, it is certainly a significant problem as well as an obstacle in the industrialization of biodiesel. The physicochemical and tri-biological properties of biodiesel are altered by oxidation during storage or usage. The effects of this phenomenon are immediately felt by the characteristics of biodiesel. However, adding different antioxidants may lessen biodiesel's sensitivity to oxidation (Bannister et al., 2011; Kumar, 2017).

According to our analysis, AAB has a water content of 0.085 , which is only slightly more than the ASTM standard. A critical component of fuel quality is its water content. Biodiesel has a higher potential to absorb moisture than conventional fuels since it is more hygroscopic and hydrophilic. High moisture levels in biodiesel encourage the growth of algae in gasoline tanks, which corrodes fuel tanks and produces slime and sludge to clog engine filters and fuel pipes, damaging the vehicle's fuel injection system (Fregolente et al., 2012).

The iodine value was determined to be 81 , which is less than the ASTM D-6751 standard. This demonstrates biodiesel's oxidative stability, saturation, and unsaturation level (Cardoso et al., 2019). AAB has a refractive index of 1.458 . It demonstrates that converting crude oil to biodiesel was successful (Lugo-Méndez et al., 2021). Additionally, we examined the carbon residue in the synthetic biodiesel that falls below the ASTM D-6751 standard.

According to this study, the HHV is 41.83 , which is within the

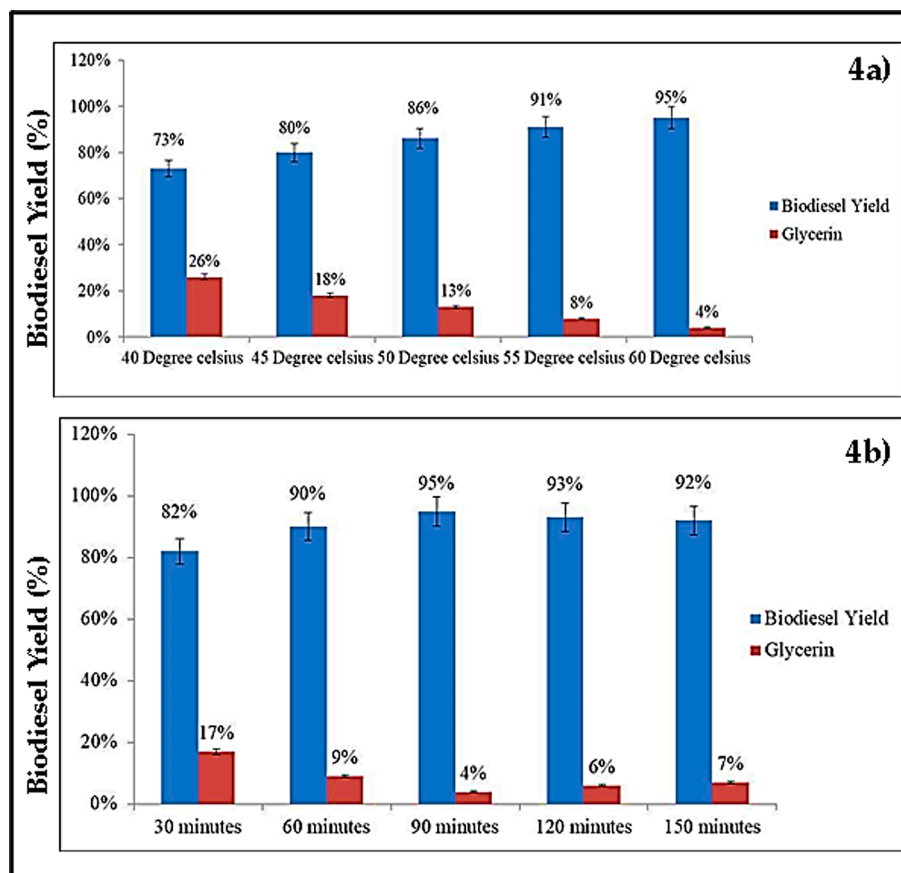


Fig. 4. A) increase in reaction temperature increases the biodiesel yield and reduces the glycerin formation; b) increase in reaction time increases the biodiesel yield and reduces the glycerin formation.

acceptable limit given by ASTM D-6751. A crucial aspect of biodiesel is its high heat value (HHV), which, like other fuel qualities, reveals details about the energy contents of the fuel as well as efficiency (Demirbaş, 2003; Marzban et al., 2022). The biodiesel's fatty acid composition, iodine concentration, and saponification value are used to compute it (Anand et al., 2010). Biodiesel has a lower HHV (39 to 43 MJ/kg) than fossil fuels (49.65 MJ/kg) (Demirbaş, 2009).

Numerous studies have shown that the fatty acid, as well as the chemical composition of non-edible biodiesels, affects the fuel properties. The fuel properties of other feedstocks are given in Table 2 (Ashraf et al., 2014).

3.6. 1H NMR spectroscopy of AAB

The singlet peak at 3.498 ppm showed that the biodiesel sample included methoxy proton ($-OCH_3$). It verifies the process of converting crude oil to biodiesel (Adewuyi et al., 2014). The existence of alpha-methylene proton ($\alpha-CH_2$) in the synthesized biodiesel was confirmed from the peaks between 2.015 and 2.062 ppm. These two peaks demonstrated that FAMES were produced from triglycerides. The presence of terminal methyl protons (CH_3) in the biodiesel was confirmed from the peaks obtained at 0.843–0.951 ppm. Peaks obtained at 1.275–1.638 ppm confirm the presence of beta-carbonyl methylene protons. At 5.189–5.426 ppm, the olefinic hydrogen indicator peaks

Table 2

Fuel properties of various commonly used feedstocks.

Vegetable oil	Density at 40 °C (kg/m ³)	Viscosity at 40 °C (mm ² /s)	Flash point (°C)	Cloud point (°C)	Pour point (°C)	Cetane number	Calorific value (MJ/kg)
Karanja (<i>Pongamia pinnata</i> L.)	876–890	4.37–9.60	163–187	13–15	–3 to 5.1	52–58	36–38
Polanga (<i>Calophyllum inophyllum</i>)	888.6–910	4–5.34	151–170	13.2–14	4.3	57.3	39.25–41.3
Mohua (<i>Madhuca indica</i>)	904–916	3.98–5.8	127–129	3–5	1–6	51–52	39.4–39.91
Rubber Seed oil (<i>Hevea brasiliensis</i>)	860–881	5.81–5.96	130–140	4–5	–8	37–49	36.5–41.07
Cotton seed	874–911	4–4.9	210–243	1.7	–10 to –15	41.2–59.5	39.5–40.1
Jajoba oil (<i>Simmondsia chinensis</i>)	863–866	19.2–25.4	61–75	6–16	–6 to 6	63.5	42.76–47.38
Tobacco oil (<i>Nicotiana tabacum</i>)	860–888.5	3.5–4.23	152–165.4	–	–12	49–51.6	38.43–39.81
Neem (<i>Azadirachta</i>)	912–965	20.5–48.5	34	–	–	51	33.7–39.5
Linseed oil (<i>Linum usitatissimum</i>)	865–950	16.2–36.6	108	1.7	–4 to –18	28–35	37.7–39.8
Jatropha (<i>Jatropha curcas</i> L.)	864–880	3.7–5.8	163–238	–	5	46–55	38.5–42

were attained (Fig. 5a) (Knothe, 2000). The successful conversion of triglycerides to biodiesel can be confirmed by these peaks (Portela et al., 2016; Ullah et al., 2020).

3.7. ^{13}C NMR study of AAB

23.92–34.21 ppm confirms the presence of long-chain ethylene carbons ($-\text{CH}_2-$) in the biodiesel. Furthermore, the presence of carbonyl carbon ($-\text{CO}$) was confirmed from the singlet peak received at 173.98 ppm. The olefinic carbons had confirmation peaks that ranged from 128.82 to 130.09 ppm. The presence of vinylic ($\text{C}=\text{H}$) substituent was confirmed by the peaks at 126.54 and 127.41 ppm (Fig. 5b). The peaks in this range for the same function groups have also been reported in other studies (Ullah et al., 2015).

3.8. Qualitative and quantitative analysis of AAB

An examination of the FAMES produced by successful transesterification was done using gas chromatography and mass spectroscopy on both a qualitative and quantitative level. According to the GC–MS data, there are 14 different types of FAMES in the AAB (Table 3). The peak of each methyl ester of fatty acid was verified using the NIST 02 library match programme. Based on the retention time, each methyl ester of a fatty acid was identified. Furthermore, it is clear from the spectrum of GC–MS that the majority of FAMES are unsaturated and thus suggest better fuel efficiency (Asci et al., 2020).

Table 3

Reported FAMES in the biodiesel sample with retention time and percentage.

S. No	Identified FAMS Compound	Retention time	Concentration in Percent
1	Myristic acid methyl ester	10.168	0.47
2	Palmitic acid methyl ester	13.424	1.36
3	Palmitoleic acid methyl ester	13.878	0.85
4	Margaric acid methyl ester	15.50	0.43
5	Heptadecenoic acid methyl ester	15.943	0.24
6	Stearic Acid methyl ester	17.897	2.41
7	Oleic Acid methyl ester	18.375	48.28
8	Elaidic acid methyl ester	18.506	0.73
9	Linoleic acid methyl ester	19.659	37.79
10	Octadecadienoic acid methyl ester	19.817	0.61
11	Linolenic acid methyl ester	21.743	4.87
12	Arachidic acid methyl ester	24.661	0.89
13	11-Eicosadienoic acid methyl ester	25.315	0.72
14	11,14,17-Eicosatrienoic fatty acid methyl ester	27.216	0.59

3.9. Fourier transform infrared analysis of AAB

FT-IR spectroscopy was used to confirm the presence of different functional groups in the biodiesel sample (Table 4 & Fig. 7). It is an effective analytical instrument for identifying the pool of macromolecular pools (such as lipids, proteins, and carbohydrates) and tracking biochemical changes in those pools (Miglio et al., 2013). FAMES are capable of absorbing electromagnetic radiation of infrared wavelengths (Atabani et al., 2019). Two principal absorption bands, the carbonyl,

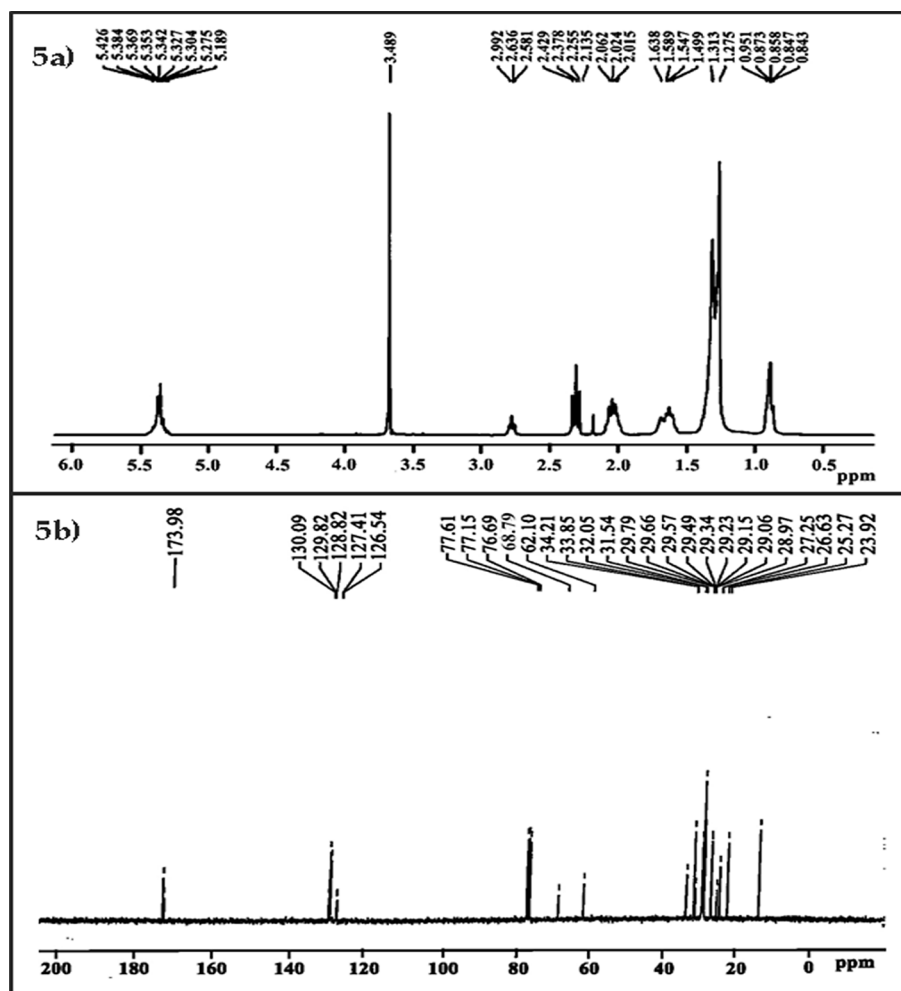


Fig. 5. Spectroscopy confirms the successful occurrence of the transesterification process a) ^1H NMR and b) ^{13}C NMR.

Table 4
Different functional groups and their peaks after FT-IR spectroscopy.

S.No.	Functional group	Corresponding peak
1	Methylene stretching	2932 cm ⁻¹
2	Methoxy stretching –O–CH ₃	2847 cm ⁻¹
3	Methoxycarbonyl (methyl ester)	1753 cm ⁻¹
4	Methyl C–H bend	1482 cm ⁻¹
5	Trimethyl	1388 cm ⁻¹
6	Methyne	1340 cm ⁻¹
7	Aromatic ether (aryl–O stretching)	1225 cm ⁻¹
8	Alkyl-substituted ether (C–O stretching)	1116 cm ⁻¹
9	Cyclic ethers C–O stretching	1060 cm ⁻¹
10	Methyne C–C vibration	977 cm ⁻¹
11	Methylene –(CH ₂) _n – rocking	763 cm ⁻¹
12	Alkyne C–H bend	683 cm ⁻¹

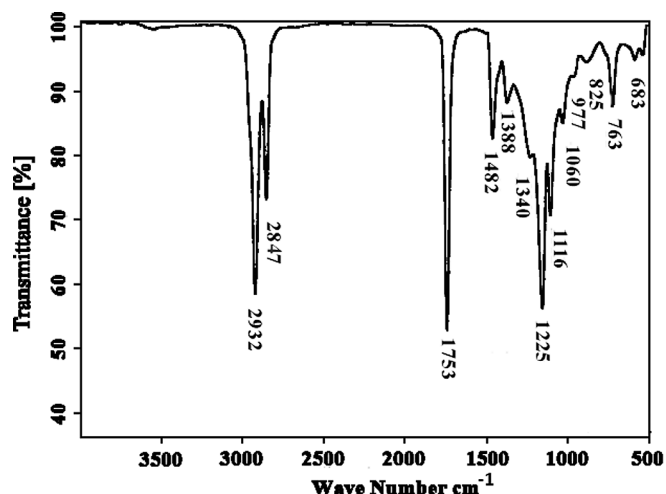


Fig. 7. FT-IR spectroscopy confirms the biodiesel formation by showing peaks for important functional groups and compounds.

with an absorption band from 1725 cm⁻¹ to 1750 cm⁻¹, and C–O, having an absorption band range of 1000–1300 cm⁻¹ are used to confirm the synthesis of esters (Ullah et al., 2020). The presence of an additional prominent distinctive absorption band at 1225 cm⁻¹ verifies aromatic ether (Siatis et al., 2006; Taufiq-Yap et al., 2014). The absorption bands detected in FT-IR spectroscopy show that the transesterification process was effective (Andrade et al., 2017; Elango et al., 2019).

4. Conclusion

Among the green and renewable energy sources available today that may fulfill the world's energy needs is biodiesel. Biodiesel, synthesized using seed oil from the inedible *Ailanthus altissima* plant, presents an attractive renewable energy solution that could potentially meet the world's energy demands. In our study, transesterification was employed to synthesize biodiesel using NiO nanoparticles as a catalyst. The optimal conditions for synthesizing biodiesel, resulting in a 95 % yield, involved a 1:24 oil-to-methanol ratio, 25 mg catalyst, 60 °C temperature, and 90 min of reaction time. The fuel's properties were assessed using ASTM methods and were found to be mostly within the accepted limits outlined in ASTM D-6751. The acid value and kinematic viscosity values of synthesized biodiesel are close to the conventional diesel, whereas it has a higher oxygen content (low calorific value) than conventional diesel. Low water content and very low sulphur content make it engine-friendly as well as eco-friendly. HHV value, cetane number, oxidative stability, and carbon residue value of biodiesel reflect its high energy content and fuel efficiency. The synthesis of the biodiesel and the chemical composition was confirmed by the use of a variety of

spectroscopic methods, including FT-IR, GC–MS, and ¹H and ¹³C NMR. Furthermore, the physico-chemical characteristics of the *Ailanthus altissima* biodiesel indicate that it is an eco-friendly fuel and a feasible option for industrial-scale biodiesel production.

Contributions of the Authors: The present work has been written with equal, direct, and intellectual contributions from all authors, who have also given their approval for publishing in this journal.

Declaration of competing interest

The authors declare that they have no known competing financial interests or personal relationships that could have appeared to influence the work reported in this paper.

Acknowledgments

The authors would like to sincerely thank the Deputyship for Research & Innovation, Ministry of Education in Saudi Arabia, for funding this research work through the Project number (IFKSUOR3-075-7) and to the Slovak Research and Development Agency (SRDA) grant APVV-22-0388. The authors also wish to acknowledge the support from the UKRI project “Advancing Creative Circular Economies for Plastics via Technological-Social Transitions” (ACCEPT Transitions, EP/S025545/1). All data is provided in full in the results section of this paper.

Funding

The Deputyship for Research & Innovation, Ministry of Education in Saudi Arabia, for funding this research work through the Project number (IFKSUOR3-075-7). It also received support from the UKRI project “Advancing Creative Circular Economies for Plastics via Technological-Social Transitions” (ACCEPT Transitions, EP/S025545/1).

References

- PAdiva, Pandey, V., Munjal, S., Ahmad, T., 2020. Structural and optical properties of sol gel synthesized NiO nanoparticles. In *AIP Conference Proceedings* (Vol. 2270, No. 1, p. 110011). AIP Publishing LLC. doi.org/10.1063/5.0020038.
- Ariyanta, H.A., Ivandini, T.A., Yulizar, Y., 2021. Novel NiO nanoparticles via phytosynthesis method: Structural, morphological and optical properties. *J. of Molec. Struct.* 1227, 129543 <https://doi.org/10.1016/j.molstruc.2020.129543>.
- Ashraf, A.M., Masjuki, H.H., Kalam, M.A., Fattah, I.R., Imtihan, S., Shahir, S.A., Mobarak, H.M., 2014. Production and comparison of fuel properties, engine performance, and emission characteristics of biodiesel from various non-edible vegetable oils: A review. *Ener. Conv. and Manag.* 80, 202–228.
- Asif, S., Ahmad, M., Bokhari, A., Chuah, L.F., Klemeš, J.J., Akbar, M.M., Yusup, S., 2017a. Methyl ester synthesis of Pistacia khinjuk seed oil by ultrasonic-assisted cavitation system. *Indust. Crops and Prod.* 108, 336–347. <https://doi.org/10.1016/j.indcrop.2017.06.046>.
- Asif, S., Ahmad, M., Zafar, M., Ali, N., 2017b. Prospects and potential of fatty acid methyl esters of some non-edible seed oils for use as biodiesel in Pakistan. *Renew. and Sust. Ener. Rev.* 74, 687–702. <https://doi.org/10.1016/j.rser.2017.02.036>.
- Birla, A., Singh, B., Upadhyay, S.N., Sharma, Y.C., 2012. Kinetics studies of synthesis of biodiesel from waste frying oil using a heterogeneous catalyst derived from snail shell. *Biores. Tech.* 106, 95–100. <https://doi.org/10.1016/j.biortech.2011.11.065>.
- Bokhari, A., Chuah, L.F., Michelle, L.Z.Y., Asif, S., Shahbaz, M., Akbar, M.M., Yusup, S., 2019. Microwave enhanced catalytic conversion of canola-based methyl ester: optimization and parametric study. *Advanced Biofuels* (pp. 153–166). Woodhead Publishing. doi.org/10.1016/B978-0-08-102791-2.00006-4.
- Chen, Z., Chen, L., Khoo, K.S., Gupta, V.K., Sharma, M., Show, P.L., Yap, P.S., 2023. Exploitation of lignocellulosic-based biomass biorefinery: A critical review of renewable bioresource, sustainability and economic views. *Biotechnology Advances* 108265.
- Chrysikou, L.P., Litinas, A., Bezergianni, S., 2022. Assessment of biodiesel stability under long-term storage and dynamic accelerated oxidation: a comparison approach. *Clean Tech. and Environ. Pol.* 24 (8), 2583–2593. <https://doi.org/10.1007/s10098-022-02335-9>.
- Dawood, S., Koyande, A.K., Ahmad, M., Mubashir, M., Asif, S., Klemeš, J.J., Show, P.L., 2021. Synthesis of biodiesel from non-edible (Brachychiton populneus) oil in the presence of nickel oxide nanocatalyst: Parametric and optimization studies. *Chemosph.* 278, 130469 <https://doi.org/10.1016/j.chemosphere.2021.130469>.
- Dharmaraj, N., Prabu, P., Nagarajan, S., Kim, C.H., Park, J.H., Kim, H.Y., 2006. Synthesis of nickel oxide nanoparticles using nickel acetate and poly (vinyl acetate) precursor.

- Mater. Sci. and Engin. b. 128 (1–3), 111–114. <https://doi.org/10.1016/j.mseb.2005.11.021>.
- Encinar, J.M., González, J.F., Sabio, E., Ramiro, M.J., 1999. Preparation and properties of biodiesel from *Cynara C arduunculus L.* oil. *Indus. & Engin. Chem. Res.* 38 (8), 2927–2931. <https://doi.org/10.1021/ie990012x>.
- Fadhil, A.B., Ahmed, K.M., Dheyab, M.M., 2017. *Silybum marianum L.* seed oil: A novel feedstock for biodiesel production. *Arab. J. Chem.* 10, S683–S690. <https://doi.org/10.1016/j.arabj.2012.11.009>.
- Ghazal, S., Akbari, A., Hosseini, H.A., Sabouri, Z., Khatami, M., Darroudi, M., 2021. Sol-gel synthesis of selenium-doped nickel oxide nanoparticles and evaluation of their cytotoxic and photocatalytic properties. *Inorgan. Chem. Res.* 5 (1), 37–49. <https://doi.org/10.22036/ICR.2020.258236.1094>.
- Guldhe, A., Moura, C.V., Singh, P., Rawat, L., Moura, E.M., Sharma, Y., Bux, F., 2017. Conversion of microalgal lipids to biodiesel using chromium-aluminum mixed oxide as a heterogeneous solid acid catalyst. *Renew. Ener.* 105, 175–182. <https://doi.org/10.1016/j.renene.2016.12.053>.
- Jan, H.A., Saqib, N.U., Khuroo, A., Sahibzada, M.U.K., Rauf, M., Alghamdi, S., Mohafez, H., 2022a. Synthesis of biodiesel from *Carthamus tinctorius L.* oil using TiO₂ nanoparticles as a catalyst. *J. King Saud Uni. Sci.* 34 (8), 102317. <https://doi.org/10.1016/j.jksus.2022.102317>.
- Jan, H.A., Šurina, I., Al-Fatesh, A.S., Almutlaq, A.M., Wali, S., Lisý, A., 2022b. Biodiesel Synthesis from Milk Thistle (*Silybum marianum (L.) Gaertn.*) Seed Oil using ZnO Nanoparticles as a Catalyst. *Energ.* 15 (20), 7818. <https://doi.org/10.3390/en15207818>.
- Jan, H.A., Osman, A.I., Šurina, I., Saleh, J., Kumar, R., Al-Fatesh, A.S., 2023. Recycling calcium oxide nanoparticles for sustainable biodiesel production from nonedible feedstock *Argemone mexicana L.* *Biofuels.* 1–10. <https://doi.org/10.1080/17597269.2023.2277989>.
- Kour, D., Rana, K.L., Yadav, N., Yadav, A.N., Rastegari, A.A., Singh, C., Saxena, A.K., 2019. Technologies for biofuel production: current development, challenges, and future prospects. *Prosp. of Renew. Bioprocess. in Future Ener. Syst.* 1–50. https://doi.org/10.1007/978-3-030-14463-0_1.
- Kuepethkaew, S., Sangkharak, K., Benjakul, S., Klomkloa, S., 2017. Optimized synthesis of biodiesel using lipase from Pacific white shrimp (*Litopenaeus vannamei*) hepatopancreas. *Renew. Ener.* 104, 139–147. <https://doi.org/10.1016/j.renene.2016.12.014>.
- Marzban, N., Libra, J.A., Hosseini, S.H., Fischer, M.G., Rotter, V.S., 2022. Experimental evaluation and application of genetic programming to develop predictive correlations for hydrochar higher heating value and yield to optimize the energy content. *J. of Environ. Chem. Engin.* 10 (6), 108880. <https://doi.org/10.1016/j.jece.2022.108880>.
- Mumtaz, M.W., Adnan, A., Mukhtar, H., Rashid, U., Danish, M., 2017. Biodiesel production through chemical and biochemical transesterification: Trends, technicalities, and future perspectives. In: *Clean Energy for Sustainable Development*. Academic Press, pp. 465–485.
- Nath, D., Singh, F., Das, R., 2020. X-ray diffraction analysis by Williamson-Hall, Halder-Wagner and size-strain plot methods of CdSe nanoparticles—a comparative study. *Mater. Chem. and Phys.* 239, 122021. <https://doi.org/10.1016/j.matchemphys.2019.122021>.
- Osman, A.I., Lai, Z.Y., Farghali, M., Yiin, C.L., Elgarahy, A.M., Hammad, A., Yap, P.S., 2023. Optimizing biomass pathways to bioenergy and biochar application in electricity generation, biodiesel production, and biohydrogen production. *Environ. Chem. Letters.* 21 (5), 2639–2705.
- Patchimpet, J., Simpson, B.K., Sangkharak, K., Klomkloa, S., 2020. Optimization of process variables for the production of biodiesel by transesterification of used cooking oil using lipase from Nile tilapia viscera. *Renew. Ener.* 153, 861–869. <https://doi.org/10.1016/j.renene.2020.02.039>.
- Rezania, S., Oryani, B., Park, J., Hashemi, B., Yadav, K.K., Kwon, E.E., Cho, J., 2019. Review on transesterification of non-edible sources for biodiesel production with a focus on economic aspects, fuel properties and by-product applications. *Ener. Conv. and Manag.* 201, 112155.
- Sebayang, A.H., Kusumo, F., Milano, J., Shamsuddin, A.H., Silitonga, A.S., Ideris, F., Chia, S.R., 2023. Optimization of biodiesel production from rice bran oil by ultrasound and infrared radiation using ANN-GWO. *Fuel* 346, 128404.
- Sladonja, B., Sušek, M., Guillermic, J., 2015. Review on invasive tree of heaven (*Ailanthus altissima (Mill.) Swingle*) conflicting values: assessment of its ecosystem services and potential biological threat. *Environ. Manag.* 56 (4), 1009–1034. <https://doi.org/10.1007/s00267-015-0546-5>.
- Suherman, S., Abdullah, I., Sabri, M., Silitonga, A.S., 2023. Evaluation of Physicochemical Properties Composite Biodiesel from Waste Cooking Oil and *Schleichera oleosa* Oil. *Energies* 16 (15), 5771.
- Takase, M., Zhang, M., Feng, W., Chen, Y., Zhao, T., Cobbina, S.J., Wu, X., 2014. Application of zirconia modified with KOH as heterogeneous solid base catalyst to new non-edible oil for biodiesel. *Energ. Conv. and Manag.* 80, 117–125. <https://doi.org/10.1016/j.enconman.2014.01.034>.
- Tan, S.X., Lim, S., Ong, H.C., Pang, Y.L., 2019. State of the art review on development of ultrasound-assisted catalytic transesterification process for biodiesel production. *Fuel.* 235, 886–907. <https://doi.org/10.1016/j.fuel.2018.08.021>.
- Taufiq-Yap, Y.H., Teo, S.H., Rashid, U., Islam, A., Hussien, M.Z., Lee, K.T., 2014. Transesterification of *Jatropha curcas* crude oil to biodiesel on calcium lanthanum mixed oxide catalyst: Effect of stoichiometric composition. *Energ. Conv. and Manag.* 88, 1290–1296. <https://doi.org/10.1016/j.enconman.2013.12.075>.
- Trifilò, P., Raimondo, F., Nardini, A., Lo Gullo, M.A., Salleo, S., 2004. Drought resistance of *Ailanthus altissima*: root hydraulics and water relations. *Tree Phys.* 24 (1), 107–114. <https://doi.org/10.1093/treephys/24.1.107>.
- Uğuz, G., Atabani, A.E., Mohammed, M.N., Shobana, S., Uğuz, S., Kumar, G., Ala'a, H., 2019. Fuel stability of biodiesel from waste cooking oil: A comparative evaluation with various antioxidants using FT-IR and DSC techniques. *Biocata. and Agricult. Biotech.* 21, 101283. <https://doi.org/10.1016/j.bcab.2019.101283>.
- Ullah, K., Jan, H.A., Ahmad, M., Ullah, A., 2020. Synthesis and structural characterization of biofuel from Cockerbur sp., using zinc oxide nanoparticle: A novel energy crop for bioenergy industry. *Frontiers in Bioengin. and Biotech.* 8, 756. <https://doi.org/10.3389/fbioe.2020.00756>.
- Yu, H., Cao, Y., Li, H., Zhao, G., Zhang, X., Cheng, S., Wei, W., 2021. An efficient heterogeneous acid catalyst derived from waste ginger straw for biodiesel production. *Renew. Ener.* 176, 533–542. <https://doi.org/10.1016/j.renene.2021.05.098>.